

Supporting Information

Binding Strength Regime Dictates Stress Relaxation Behavior

Ipek Sacligil, Christopher W. Barney,[†] Alfred J. Crosby, Gregory N. Tew*

Department of Polymer Science and Engineering, University of Massachusetts, Amherst, Massachusetts, 01003, United States

[†] Present address: Materials Research Laboratory, Department of Mechanical Engineering, and Department of Chemical Engineering, University of California, Santa Barbara, CA 93106.

*Corresponding Author: tew@mail.pse.umass.edu

Table of Contents

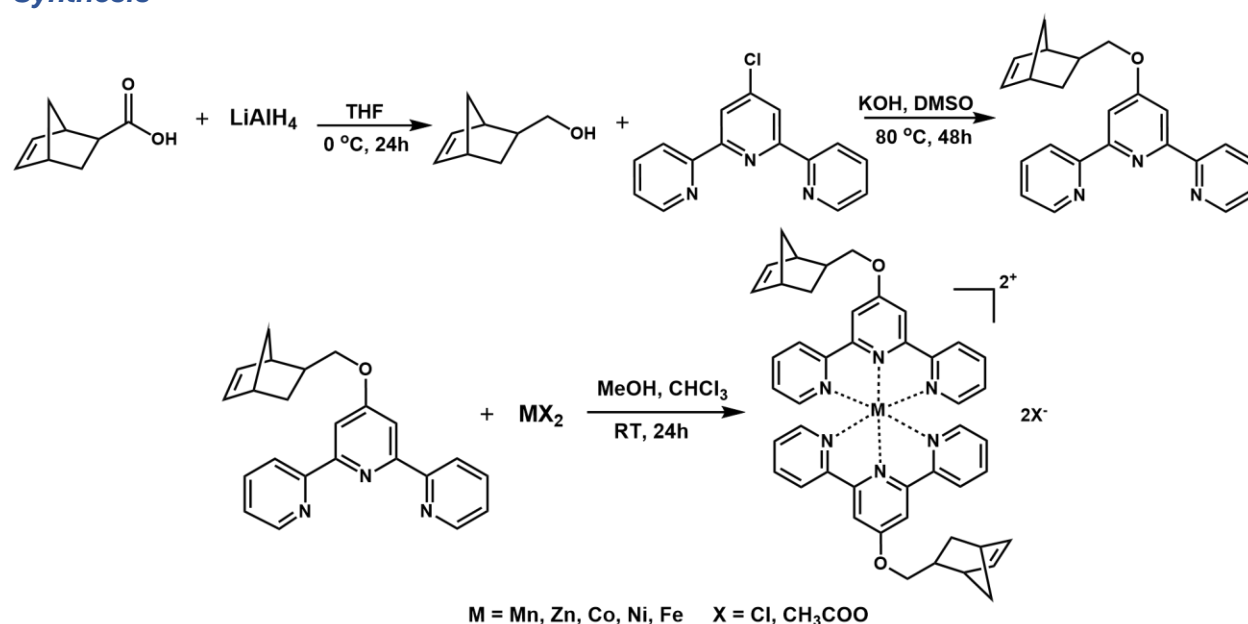
Section 1: Experimental	1
<i>Materials</i>	1
<i>Synthesis</i>	1
<i>Instrumentation</i>	3
Section 2: Measuring stress-relaxation time via rheology and indentation	3
Section 3: Additional stress relaxation curves	4
<i>Fitting with a Single Exponential Decay Function</i>	5
Section 4: Testing for poroelasticity/ viscoelasticity	7
Section 5: Wide angle X-ray scattering for ion clustering	8
Section 6: Effect of quenching G2 catalyst	8
Section 7: Effects of counterion on stress-relaxation	9
Section 8: Effects of crosslink density and bond strength regimes	9
<i>Bond Strength Regimes</i>	10
<i>Distance between Two Stickers</i>	10
<i>Moduli of Various Networks with Varying Crosslink Densities</i>	11
Section 9: Extension of the crosslink density independent stress relaxation time theory to other systems	11
References	12

Section 1: Experimental

Materials

Tetrahydrofuran (Fisher Scientific) was dried over sodium under N_2 and then distilled before use. Exo-5-norbornene-2-carboxylic acid, lithium aluminum hydride ($LiAlH_4$), potassium hydroxide (KOH), 4-chloro-2,2':6',2''-terpyridine, zinc (II) chloride, manganese (II) chloride, iron (II) chloride tetrahydrate, nickel(II) chloride hexahydrate, cobalt(II) chloride, ruthenium(III) chloride hydrate, zinc (II) acetate, cobalt (II) acetate tetrahydrate, Grubbs' 2nd generation catalyst (G2), N-ethylmorpholine, dihydroxyl-terminated poly(ethylene glycol) (PEG), triphenyl phosphine, diisopropyl azodicarboxylate (DIAD), dichloromethane (DCM), chloroform, dimethyl sulfoxide (DMSO) and methanol were purchased from Sigma Aldrich, Alfa Aesar, Acros Organics, Fisher Scientific, Ambeed, or Tokyo Chemical Industry and were used as received.

Synthesis



Scheme S1. Synthetic scheme for norbornene terpyridine and bis(norbornene terpyridine) metal salt complex

Synthesis of 5-norbornene-2-methanol. Exo-5-norbornene-2-methanol was synthesized following previously published procedures.^{1,2} Exo-5-norbornene-2-carboxylic acid (2.5 g, 18.1 mmol) was dissolved in dry THF (60 ml) and cooled in an ice bath. Lithium aluminum hydride solution in THF (2.4 M, 5.6 mL) was added dropwise to the solution. The reaction was stirred overnight letting the solution to warm up room temperature slowly. The flask was then cooled down and the reaction solution was quenched with RO water. The precipitated salt was filtered and THF was evaporated by rotary evaporator. The remaining viscous liquid was diluted with water and extracted with chloroform. The chloroform phase was collected and dried over Na_2SO_4 , the pure product was obtained as a clear yellow liquid (80% yield) by evaporating the chloroform *in vacuo*. 1H NMR (500 MHz, $CDCl_3$) 6.10 (2H, m), 3.71 (1H, m), 3.55 (1H, m), 2.83 (1H, s), 2.76 (1H, s), 1.62 (1H, m), 1.37-1.20 (3H, m), 1.12 (1H, m).

Synthesis of norbornene-functionalized terpyridine. Norbornene terpyridine was synthesized by adapting previous studies.^{1,2} Exo-5-norbornene-2-methanol (2 g, 16 mmol) was added to a

flask containing KOH (2.6g, 46 mmol) in DMSO (50 mL). The flask was heated to 80 °C for 2 hours. 4'-chloro-2,2':6',2"-terpyridine (2.16 g, 8.1 mmol) dissolved in 50 mL DMSO by heating to 80 °C for 2 hours and then added to the flask containing *exo*-5-norbornene-2-methanol and stirred for 48 hours at 80 °C. After cooled down, the solution was precipitated in ice water (900 mL) and the product was extracted with ethyl acetate. The ethyl acetate phase was dried over Na₂SO₄ and removed in vacuo. The product was recrystallized from methanol and obtained as light brown crystals (68% yield). ¹H NMR 8.72 (2H, s), 8.65 (2H, s), 8.07 (1H, s) 7.90 (2H, m), 7.37 (2H, m), 6.15 (2H, m), 4.32 (1H, m), 4.15 (1H, m), 2.91 (2H, s), 1.97 (1H, m), 1.41 (4H, m).

Synthesis of bis(norbornene terpyridine) metal salt complexes. Metal-terpyridine complexes were synthesized by adapting previously published literature.^{2,3} All metal complexes except bis(norbornene terpyridine) ruthenium chloride were synthesized following the same procedure. Bis(norbornene terpyridine) iron chloride is given as an example. Norbornene terpyridine (0.2 g, 0.562 mmol) was dissolved in chloroform (10 mL), and FeCl₂·4H₂O (56 mg, 0.282 mmol) was dissolved in methanol (10 mL). The solution containing FeCl₂·4H₂O was then added into chloroform and the solution turned dark violet very quickly. After 8 hours, the solvent was removed in vacuo. The product was dried and obtained as a violet powder under vacuum. It was used as-is without further purification. ¹H NMR (500 MHz, MeOD), 8.76 (4H, s), 8.67 (4H, m), 7.93 (4H, m), 7.26 (4H, m), 7.16 (4H, m), 6.27 (4H, m), 4.74 (4H, m), 3.10 (2H, s), 3.02 (2H, s), 2.20 (2H, m), 1.64 (2H, m), 1.55 (6H, m).

Synthesis of bis(norbornene terpyridine) ruthenium chloride complex. Bis(norbornene terpyridine) ruthenium chloride was synthesized as described in the literature.² Norbornene terpyridine (0.6 g, 1.68 mmol) and RuCl₃·H₂O (0.172 g, 0.83 mmol) were dissolved in 150 mL methanol and stirred under reflux. After 2 hours, N-ethyl morpholine (0.176 mL, 0.69 mmol) was added dropwise and the reaction was stirred under reflux overnight. The methanol was removed in vacuo, the obtained red solid was washed with water and chloroform to dissolve unreacted RuCl₃·H₂O and norbornene terpyridine, respectively. The product was dried under vacuum to obtain red powder. ¹H NMR (500 MHz, MeOD) 8.70 (4H, m), 8.59 (4H, m), 7.95 (4H, m), 7.50 (4H, m), 7.24 (4H, m), 6.26 (4H, m), 4.64 (2H, m), 4.51 (2H, m), 3.06 (2H, m), 3.00 (2H, m), 2.15 (2H, m), 1.61 (2H, m), 1.54 (6H, m).

Synthesis of metal-ligand networks. Poly(bis(norbornene terpyridine) iron chloride-co-norbornene) with 10 mol% crosslinks is given as an example: Norbornene (90 mg, 0.956 mmol) was dissolved in 0.3 mL of chloroform and bis(norbornene terpyridine) iron chloride (88.96 mg, 0.106 mmol) was dissolved in 0.3 mL chloroform and 0.35 mL methanol. The reagents were mixed and Grubbs' catalyst 2nd generation (6 mg, 0.007 mmol) dissolved in 0.2 mL chloroform was added to the reagents. The reaction mixture was swirled to mix the reagents right after G2 addition and let it react for 30 minutes before indentation experiments.

Synthesis of covalent control network. Poly(ethylene glycol) thiol-ene network was synthesized from the procedure from our group.^{4,5} The norbornene end-functionalized PEG (*M_n*= 4,000 g/mol) precursor (100 mg, 0.025 mmol), pentaerythritol tetrakis(3-mercaptopropionate) (PETMP) (6.3 mg, 0.013 mmol), and 2-hydroxy-4'-(2-hydroxyethoxy)-2-methyl-propiofenone as photoinitiator (1.1 mg) were dissolved in DMF (1 mL). The precursor solution was put into a vial suitable for indentation tests the desired mold and then irradiated with 365 nm light from a Blak-Ray 100 W B-110 AP/R lamp for thirty minutes.

Instrumentation

Nuclear Magnetic Resonance (NMR). The ^1H NMR spectra were recorded using a Bruker 500 MHz in CDCl_3 or MeOD. The NMR facilities are maintained by University of Massachusetts, Amherst and directed by Dr. Weiguo Hu.

Indentation experiments. Flat-punch indentation experiments were performed on Stable Microsystems TA.XT plus Texture Analyzer with a 50N load cell. Flat, cylindrical steel probes of 0.76 or 2 mm in diameter were used to indent the networks at 1 mm/s until the force of ~ 10 or ~ 20 mN was reached. The networks were allowed to relax until the force reaches zero or stays stable.

Compliance (C) is found from the ratio of displacement over force and used in the following equation from Shull and coworkers to calculate the modulus:

$$\text{Modulus} = \frac{3}{8C \left[1 + 1.33 \left(\frac{a}{h} \right) + 1.33 \left(\frac{a}{h} \right)^3 \right]} a$$

Where a is contact radius and h is the height of the sample, typically between 9-11 mm for the networks in this study.⁶

X-ray scattering. All wide-angle X-ray scattering (WAXS) testing was performed using Ganesha SAXS-LAB with $\text{Cu K}\alpha$ radiation ($\lambda = 0.154$ nm) under vacuum with an incident beam diameter of 0.3 mm. The dried metal-ligand networks were cut thinly, put on a X-ray washer and secured with Kapton tape. WAXS measurements were conducted at room temperature on samples roughly 1 mm thick. The samples were loaded onto the sample holder and secured with Kapton tape. The samples were then irradiated for 360 s.

Rheology. Shear rheological experiments were performed on stress-controlled TA Instruments AR2000 with an environmental test chamber. Measurements were carried out at room temperature using 25-mm aluminum ETC plates. First, a stress sweep was recorded at frequency of 1 Hz to determine the linear region. Then, a frequency sweep was recorded at constant oscillation stress of 60 Pa and a frequency range of 0.01-100 Hz.

Section 2: Measuring stress-relaxation time via rheology and indentation

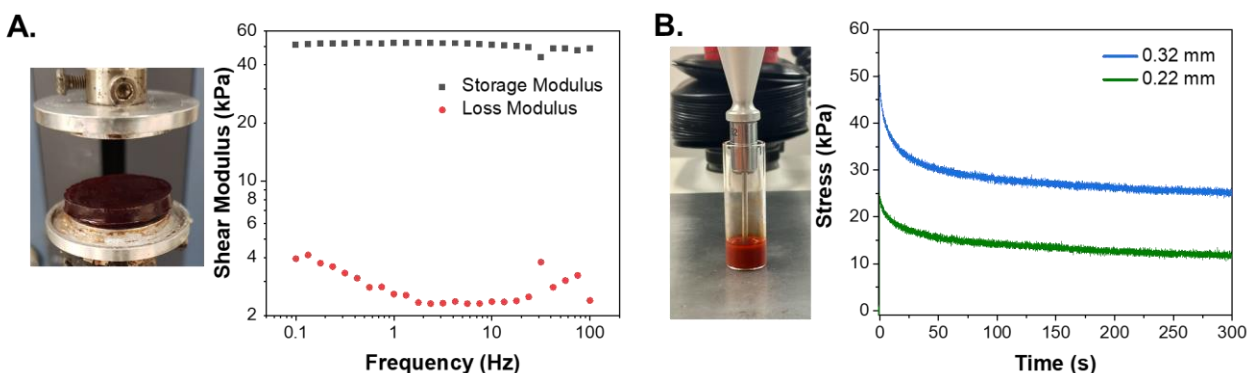


Figure S1 (A) Picture of RuCl_2 network and the frequency sweep between 0.1-100 Hz. Both storage (gray squares) and loss (red circles) moduli are frequency-independent and no crossover frequency was observed in this frequency range. (B) Picture of flat punch indentation test of RuCl_2 network and stress-

relaxation curves for RuCl_2 network at different indentation depths, 0.32 mm (blue) and 0.22 mm (green). The load was divided by the indenter area to calculate stress.

Section 3: Additional stress relaxation curves

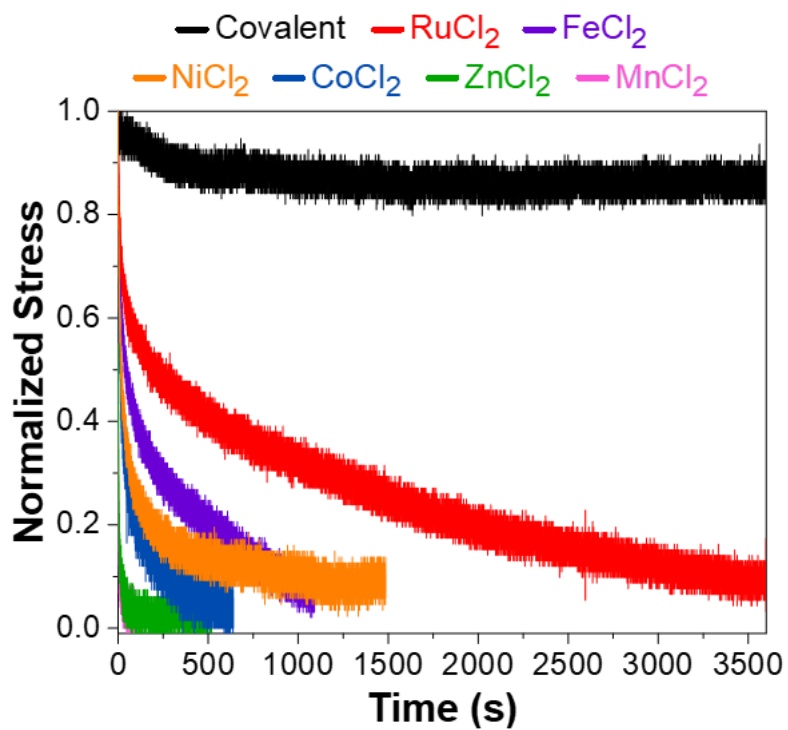


Figure S2. Full stress-relaxation curves of RuCl_2 (red), FeCl_2 (purple), NiCl_2 (orange), CoCl_2 (blue), ZnCl_2 (green), MnCl_2 (pink), and covalent network (black). The stress was normalized by the maximum value in that dataset. The data was shifted to reach maximum force at zero seconds.

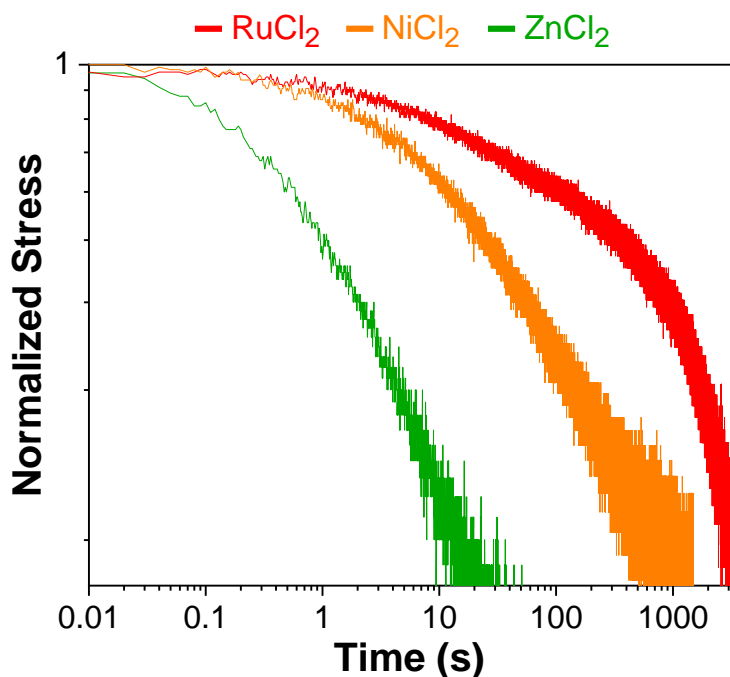


Figure S3. Full stress-relaxation curves of **RuCl₂** (red), **NiCl₂** (orange), **ZnCl₂** (green) in a log-log plot

Fitting with a Single Exponential Decay Function

Reconfigurable networks with various metal centers were fitted with a single exponential decay in OriginPro 2020 software following the form of:

$$\frac{\sigma}{\sigma_0} = A * \exp(-t/\tau) + y_0$$

where σ/σ_0 is normalized stress (dependent parameter), A is the amplitude, t is the time (independent parameter), τ is the stress relaxation time and y_0 is the offset. The fit parameters were reported as calculated by Origin software. Since the data collection was stopped when stress dissipation stabilizes or reaches 90%, an offset was introduced. As a result, a parameter of amplitude was also introduced to balance the equation. Rather than the full stress relaxation curves, certain data points were chosen to apply the fit to circumvent overwhelming amount of data points as the time gets longer.

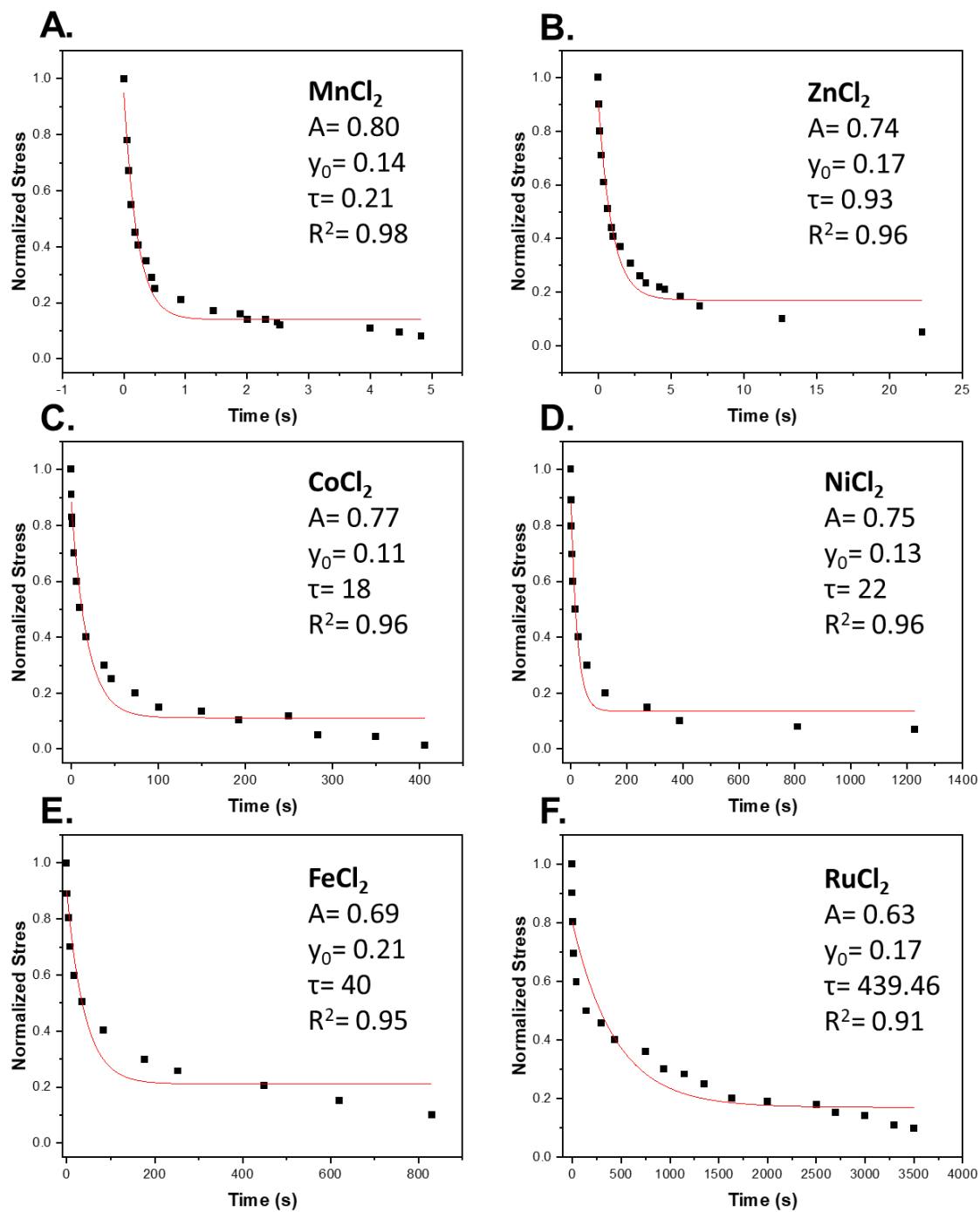


Figure S4. Single exponential fits for (A) MnCl₂, (B) ZnCl₂, (C) CoCl₂, (D) NiCl₂, (E) FeCl₂, and (F) RuCl₂ where A, τ , γ_0 and R-square are given in inset.

For slower networks, a more complex stress relaxation process might be involved as can be seen by decreasing R^2 values. However, single exponential decay allows us to compare relaxation time of all networks quantitatively and R^2 values stay above 0.9 showing acceptable level of correlation.

Section 4: Testing for poroelasticity/ viscoelasticity

Tests for poroelasticity and viscoelasticity have been done using existing literature.⁷⁻⁹ Either both stress and time or only stress was normalized for stress relaxation curves measured with different probe sizes. If normalizing only stress leads to collapse of the curves, this indicates the system follows viscoelasticity. Whereas, if normalizing both stress and normalizing the time by probe size collapses curves into a single curve, poroelasticity dominates the stress-relaxation behavior. Normalized curves for ZnCl_2 and FeCl_2 are shown as an example:

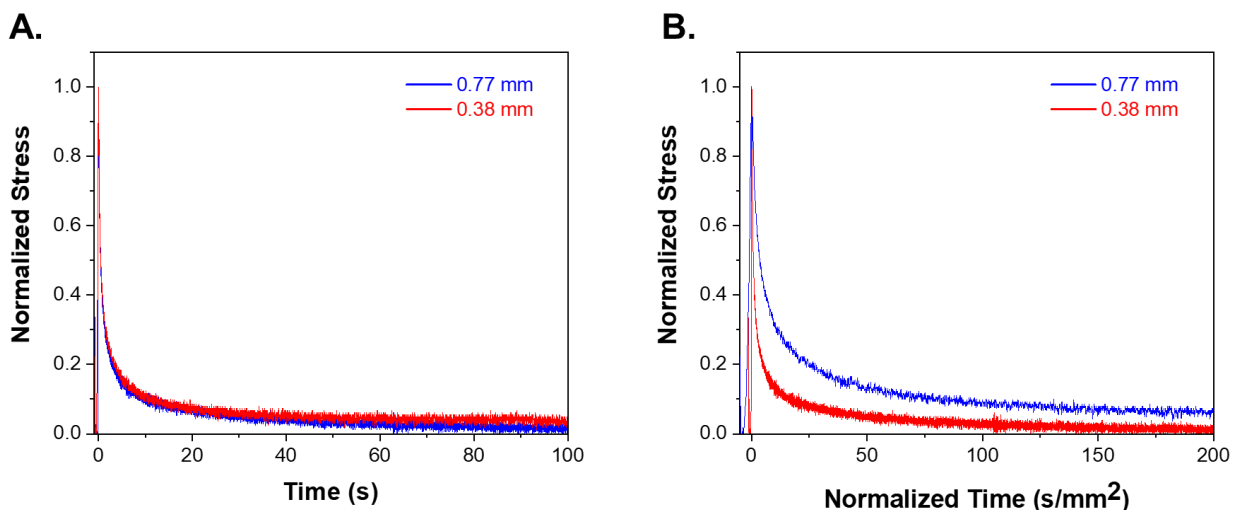


Figure S5. (A) Stress relaxation curves of ZnCl_2 with two different probe sizes ($r = 0.77$ or 0.38 mm). Only stress was normalized by the maximum stress value in that dataset. (B) Stress-relaxation curves of ZnCl_2 with two different probe sizes ($r = 0.77$ or 0.38 mm). Stress was normalized by the maximum value in that dataset and time was normalized by probe size area.

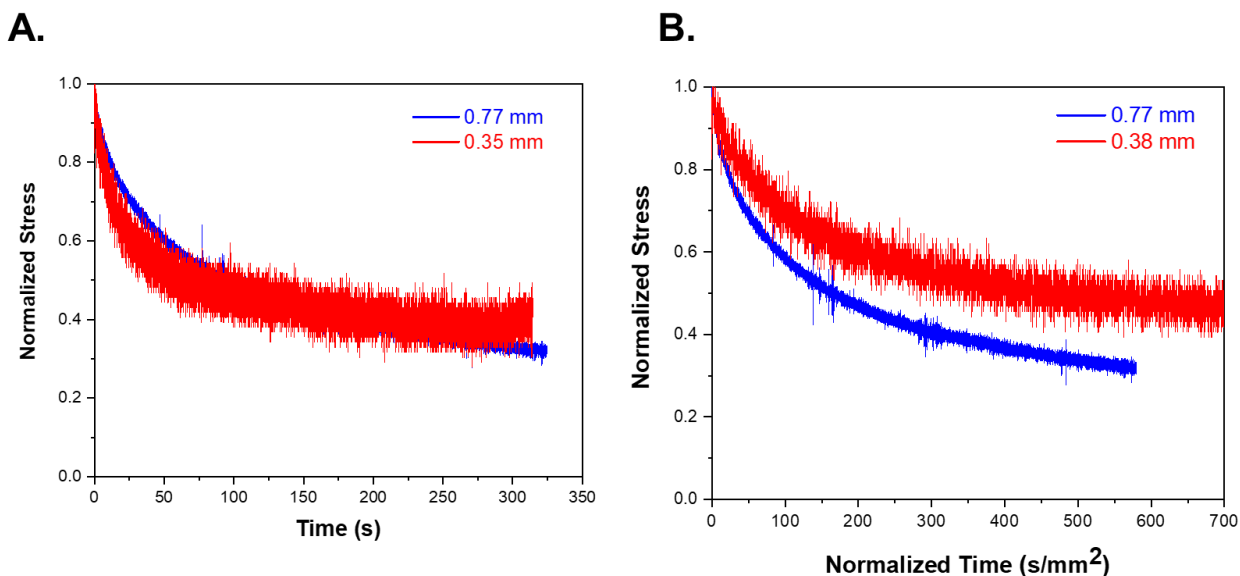


Figure S6. (A) Stress-relaxation curves of RuCl_2 with two different probe sizes ($r = 0.77$ or 0.38 mm). Only stress was normalized by dividing the dataset by the maximum stress value in that dataset. (B) Stress-

relaxation curves of **RuCl₂** with two different probe sizes ($r = 0.77$ or 0.38 mm). Time was also normalized by probe size area.

Section 5: Wide angle X-ray scattering for ion clustering

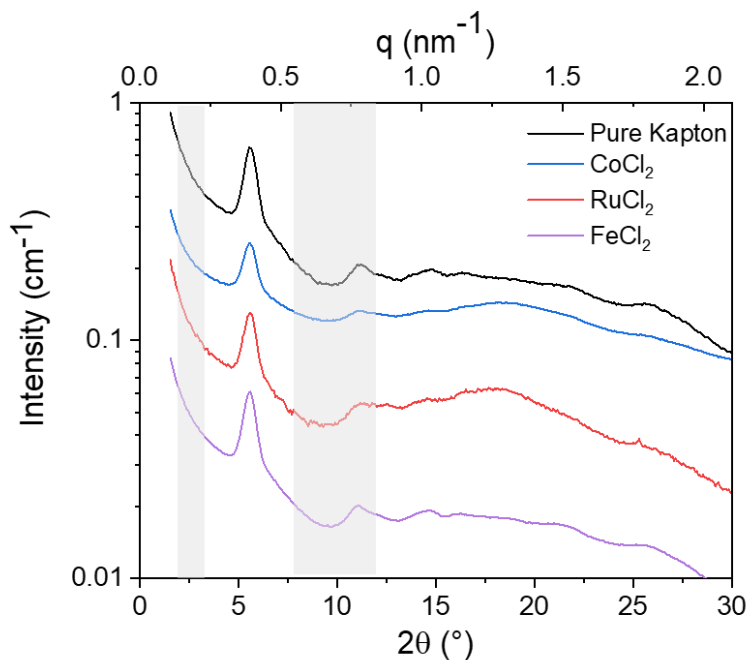


Figure S7. WAXS profiles of **CoCl₂**, **RuCl₂**, and **FeCl₂** networks. The shaded areas correspond to the regions that ion clustering was observed in earlier studies.^{2,10,11}

Section 6: Effect of quenching G2 catalyst

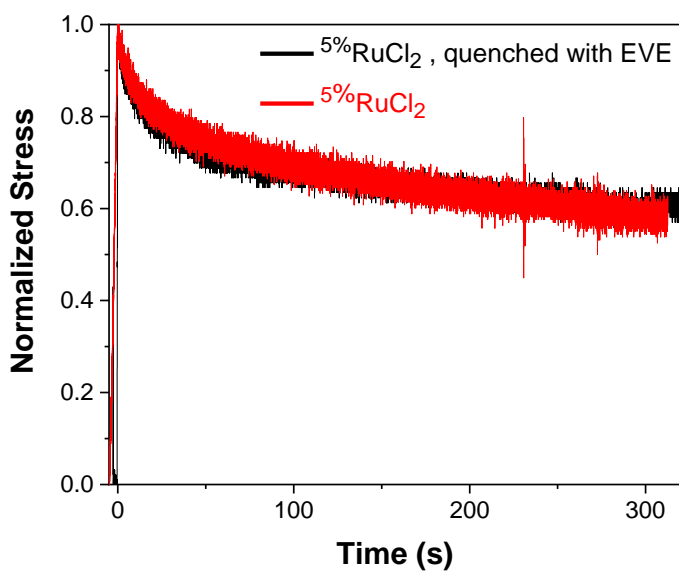


Figure S8. Stress relaxation curves of $5\% \text{RuCl}_2$ where G2 was quenched with ethyl vinyl ether (black), $5\% \text{RuCl}_2$ network where G2 catalyst was not quenched with EVE (red). These curves show that additional metathesis from unquenched G2 catalyst does not contribute to stress relaxation.

Section 7: Effects of counterion on stress-relaxation

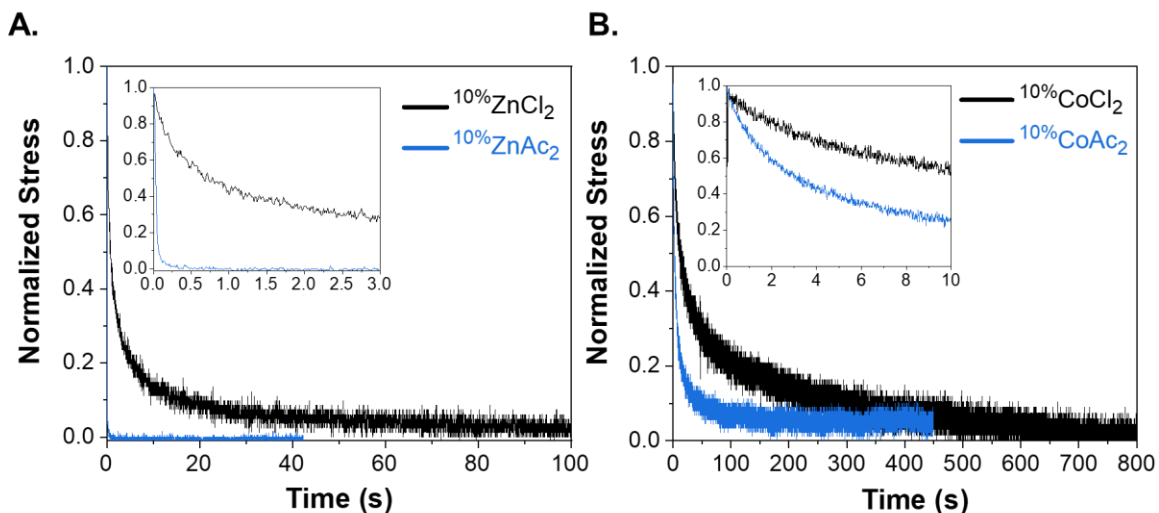


Figure S9. (A) Stress relaxation curves of network with 10% bis(norbornene terpyridine) zinc chloride crosslinks, named as $10\% \text{ZnCl}_2$ (black), and with 10% bis(norbornene terpyridine) zinc acetate crosslinks named as $10\% \text{ZnAc}_2$ (blue). Inset shows the early relaxation time 0-3 seconds for both $10\% \text{ZnCl}_2$ and $10\% \text{ZnAc}_2$. (B) Stress-relaxation curves of network with 10% bis(norbornene terpyridine) cobalt chloride crosslinks, named as $10\% \text{CoCl}_2$ (black), and with 10% bis(norbornene terpyridine) cobalt acetate crosslinks named as $10\% \text{CoAc}_2$ (blue). Stress relaxation data was collected by flat-punch indentation with an indenter radius of 0.36 mm and a preset load of ~ 10 mN. The data was shifted to reach maximum force at 0 seconds. The stress was normalized by the maximum value in that dataset.

Section 8: Effects of crosslink density and bond strength regimes

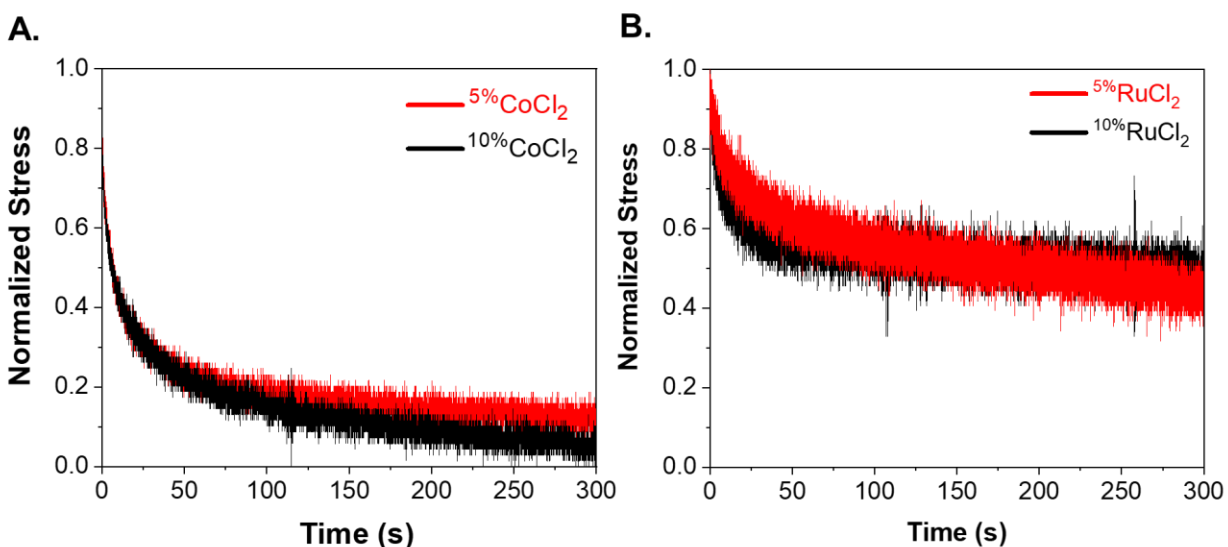


Figure S10. (A) Stress-relaxation curves of 10%**CoCl₂** (black), 5%**CoCl₂** (red) (B) Stress-relaxation curves of network with 10% bis(norbornene terpyridine) cobalt chloride crosslinks, named as 10%**RuCl₂** (black), 5%**RuCl₂** (red). Stress-relaxation data was collected by flat-punch indentation with an indenter radius of 0.36 mm and a preset load of 10 mN. The data was shifted to reach maximum force at 0 seconds. The stress was normalized by the maximum value in that dataset.

Bond Strength Regimes

$$k_b T \ln N < \varepsilon < 2k_b T \ln N \quad (\text{Intermediate regime})$$

$$2k_b T \ln N < \varepsilon \quad (\text{Strong regime})$$

For our systems, number of monomers per dangling chain, N, was taken as number of monomers between crosslinks.

N= 9 for 10 mol% crosslinks, N= 19 for 5 mol% crosslinks, N=39 2.5 mol% crosslinks

Hence, for intermediate regime the network should satisfy the condition of:

$$5.7 < E_d < 11.4 \text{ kJ/mole}$$

Bond strength of iron-, nickel- and cobalt-terpyridine interactions in water were reported as 120, 87, 61 kJ/mol respectively.¹² These reported numbers were considered as a close representation of our system and indicated all these metal centers will be in the strong regime (bond strengths are higher than 11.4 kJ/mol).

The lowest reported value for bond strength of metal-terpyridine interactions was 45 kJ/mole for terpyridine-zinc nitrate. This value was taken as the upper limit of the value of terpyridine-zinc acetate interaction as there are no reports measuring the bond strength.

The root mean squared distance between two open stickers Δr_{open} was calculated as following:¹³

Total sticker concentration, c_t for 10 mol% crosslinks: $c_t = 0.082 \text{ M}$

$$c_{\text{open}} \approx (c_t / (2K_{\text{eq}}))^{1/2}$$

$$\Delta r_{\text{open}} = c_{\text{open}}^{-1/3}$$

Metal Center	Log (K_f) ¹²	Log (K_d) ¹²	Log (K_{eq})	Δr_{open} (nm)
Fe(tpy) ₂	7.0	-6.8	13.8	455.6
Ni(tpy) ₂	5.3	-5.8	11.1	163.3
Co(tpy) ₂	6.7	-3.2	9.9	103.54
Zn(tpy)	6.1	0.1	6.0	< 23.5

Table S1. Formation rate constant (K_f), dissociation rate constant (K_d), equilibrium constants of metal-terpyridine complexes (K_{eq}) and the root mean squared distance between two open stickers

Distance between Two Stickers

The distance between two stickers was calculated by drawing the monomer units in Avogadro software and measuring the distance between them. Lowest energy configuration for the molecule was applied before the distance measurement. For 10% crosslinks, this value was multiplied by 9 to get distance between two stickers.

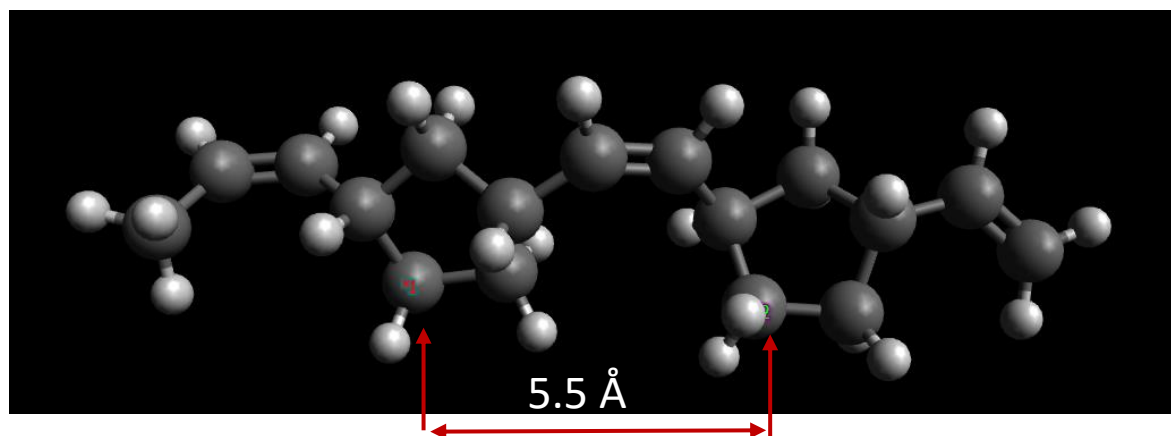


Figure S11. Calculation of the distance between stickers by using Avogadro™ software. Poly(norbornene) backbone was drawn and the geometry was optimized. Then, the distance was measured with 'click to measure' tool.

Moduli of Various Networks with Varying Crosslink Densities

Network	Elastic Modulus (kPa)		
	2.5% crosslinks	5% crosslinks	10% crosslinks
CoCl ₂		14	19
ZnCl ₂		9	30
MnCl ₂	7	9	32

Table S2. Moduli of various networks at different crosslink densities

Section 9: Extension of the crosslink density independent stress relaxation time theory to other systems

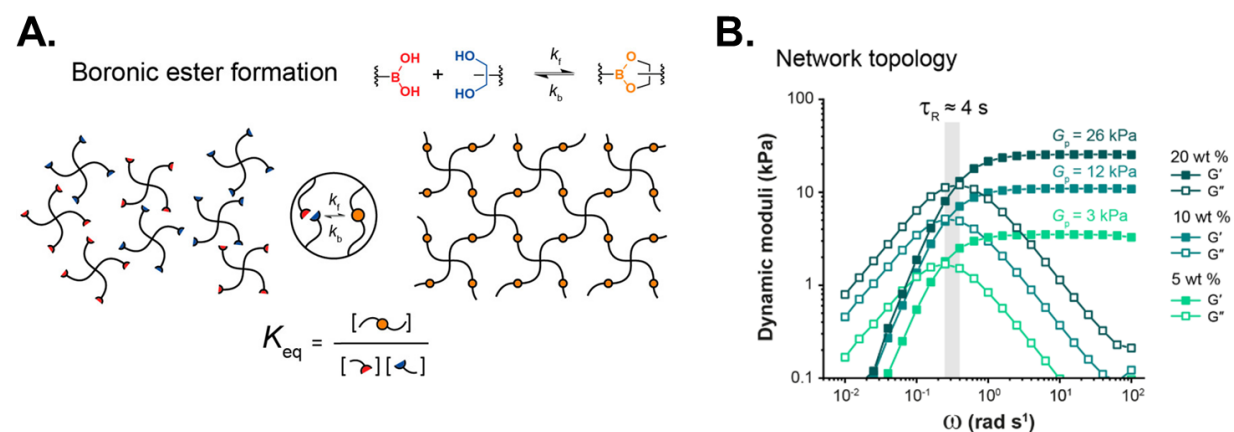


Figure S12. (A) Boronic ester-based tetra-arm hydrogels formed via reversible covalent bonding between boronic acid (red) and diol (blue), forming dynamic boronic esters (orange). (B) The plateau modulus of boronic ester-based hydrogels, G_p , varied with the polymer content (wt%) of the gels (PEG-PBA/GL, pH 8; $\gamma = 1\%$). The figure shows that the change in crosslink density does not affect the stress relaxation time in boronic ester networks. The figure was republished in part permission from the American Chemical Society.¹⁴

Intermediate regime constraints for this system were calculated for a four-arm PEG macromonomer with molecular weight of 10,000 g/mol

$$N_c = \frac{10,000 \text{ g/mol}}{44.05 \text{ g/mol} \times 4 \text{ arms}} = 114$$

$k_B T \ln N < E_a < 2k_B T \ln N_c$ for $\ln(114)$

$11.7 < E_d < 23.4 \text{ kJ/mol}$

Activation energy for gluconolactone used by Tibbit and coworkers could not be measured due to build up at intermediate temperatures.¹⁵ Therefore, we took an average of the activation energies measured for boronic esters by hydrolysis. Calculated average of 26.5 kJ/mol that indicates these networks are in strong binding strength regime for studied parameters.¹⁵

References

- 1 Y. Zha, M. L. Disabb-Miller, Z. D. Johnson, M. A. Hickner and G. N. Tew, *J. Am. Chem. Soc.*, 2012, 4493–4496.
- 2 M. T. Kwasny, L. Zhu, M. A. Hickner and G. N. Tew, *J. Polym. Sci. Part A Polym. Chem.*, 2018, **56**, 328–339.
- 3 M. T. Kwasny, L. Zhu, M. A. Hickner and G. N. Tew, *J. Am. Chem. Soc.*, 2018, **140**, 7961–7969.
- 4 J. Cui, M. A. Lackey, A. E. Madkour, E. M. Saffer, D. M. Griffin, S. R. Bhatia, A. J. Crosby and G. N. Tew, *Biomacromolecules*, 2012, **13**, 584–588.
- 5 J. Cui, M. A. Lackey, G. N. Tew and A. J. Crosby, *Macromolecules*, 2012, **45**, 6104–6110.
- 6 K. R. Shull, D. Ahn, W. Chen, C. M. Flanigan and A. J. Crosby, 1998, **511**, 489–511.
- 7 R. M. Delaine-Smith, S. Burney, F. R. Balkwill and M. M. Knight, *J. Mech. Behav. Biomed. Mater.*, 2016, **60**, 401–415.
- 8 Q. W. Anirudh, C. M. Michelle and L. O. X.-H. Z. Zhao, *Acta Mech. Sin.*, 2014, **30**, 20–27.
- 9 Z. I. Kalcioğlu, R. Mahmoodian, Y. Hu, Z. Suo and K. J. Van Vliet, *Soft Matter*, 2012, **8**, 3393–3398.
- 10 D. Chen and M. A. Hickner, *Macromolecules*, 2013, **46**, 9270–9278.
- 11 S. Bode, M. Enke, R. K. Bose, F. H. Schacher, S. J. Garcia, S. Van Der Zwaag, M. D. Hager and U. S. Schubert, *J. Mater. Chem.*, 2015, 22145–22153.
- 12 R. Hogg and R. G. Wilkins, *J. Chem. Soc.*, 1962, **2**, 341–350.
- 13 E. B. Stukalin, L. H. Cai, N. A. Kumar, L. Leibler and M. Rubinstein, *Macromolecules*, 2013, **46**, 7525–7541.
- 14 B. Marco-Dufort, R. Iten and M. W. Tibbitt, *J. Am. Chem. Soc.*, 2020, **142**, 15371–15385.
- 15 B. Kang and J. A. Kalow, *ACS Macro Lett.*, 2022, **11**, 394–401.